Observation of Intense Filaments in Fully Developed Turbulence

F. Belin, J. Maurer, P. Tabeling, H. Willaime

Observation of Intense Filaments in Fully Developed Turbulence

F. Belin, J. Maurer, P. Tabeling (*) and H. Willaime

Laboratoire de Physique Statistique, École Normale Supérieure (**), 24 rue Lhomond, 75231 Paris Cedex 05, France

(Received 3 May 1995, revised 10 November 1995, accepted 3 January 1996)

PACS.47.27.Gs – Isotropic turbulence; homogeneous turbulence
PACS.47.27.Jv – High-Reynolds-number turbulence

Abstract. — We study the structure of the large events which control the tails of the pdf of the velocity derivatives in an helium experiment. For $R_\lambda < 700$, we find that these events have a remarkable structure, which is consistent with that of intense vortex filaments ("worms") observed previously in numerical studies. The characteristics of such objects (form, size and circulation distributions, scaling with the Reynolds number) are in good agreement with reported numerical findings. These objects do not contribute significantly to the overall dissipation but they control an important part of the intermittency in the inertial range. Above $R_\lambda \approx 700$, the structure of such events dramatically changes; we interpret this observation as an instability. We finally offer a physical interpretation of a previous experiment showing that around $R_\lambda \approx 700$, the flatness of the velocity derivatives shows a transitional behaviour.

1. Introduction

The small scale structure of fully developed turbulence is a major issue which has been discussed at length for at least three decades [1]. Much progress has been done on the subject these last four years, and we now have some crucial informations, coming both from numerical simulations and real experiments. It has been shown, in numerical experiments [2], that the small scale structure of turbulence includes intense filaments, named "worms". These objects turn out to control the tails of the pdf (probability density function) of the vorticity distribution, so that they play an important role in the determination of quantities such as the flatness and hyperflatness factors of the velocity derivatives, which depend on the characteristics of such tails. Concerning the low order moments of the velocity gradients, such as the dissipation, their contribution is found to be small. To the best of our knowledge, their influence on the inertial range intermittency has not been investigated so far. On the (physical) experimental side, vortex filaments have been identified in a counter rotating disk experiment, by using bubble visualization technique [3], pressure fluctuations measurements [4] and studying the correlations between local pressure and velocity [5]. According to [5], one can define a primary population of vortex filaments with sizes extending from the Taylor to the dissipative scale, and resulting from the partial rollup of stretched shear layers; there also exists a second population

(*) Author for correspondence
(**) Laboratoire associé au CNRS, à l'ENS, aux Universités Paris 6 et Paris 7.

of filaments, which results from the instability of the first one. These are smaller, and they may correspond to the worms observed in the numerical studies.

In the present experiment, which is a low temperature flow of helium gas driven between two counter-rotating disks, we investigate the structure of the events which control the tails of the velocity derivatives. We shall show that these events can be reasonably identified as the worms previously found in numerical simulations. Once they are identified, their contribution can be isolated and analyzed. As the Reynolds number increases, we observe that, above a certain threshold, the structure of such objects abruptly changes, suggesting instability. These observations allow to offer a physical interpretation of previous results obtained on the same system [6], and which showed that the flatness factor of the velocity derivatives shows a transitional behaviour around the same threshold value of the Reynolds number.

2. Experimental Set-Up

Since the two set-ups we use have been described elsewhere [7], we give here a brief presentation of them. The flow is confined in a cylinder, which is limited axially by two counter-rotating disks, driven by DC motors. There are two set ups: in the larger one (cell 2), the working volume is 10 cm in radius, 13.1 cm high, and in the smaller one (cell 1), it is 3.3 cm in radius and 5.5 cm in height. The two cells have thus slightly different aspect ratio height over radius — 0.60 and 0.76 respectively for cell 1 and 2. Each cell is enclosed in a cylindrical vessel, in thermal contact with a liquid helium bath. The temperature of the experiment is regulated at a constant value, comprised between 4.2 to 8 K. The vessel is filled with helium gas, at a controlled pressure, ranging from 0 up to 6 atm. The thermal stability is remarkable: in the working volume, the root mean square of the local thermal fluctuations does not exceed 1 mK.

In both cases, the local velocity is measured by "hot"-wire anemometers, made from a 7 μm thick carbon fiber, stretched across a rigid frame; a metallic evaporation covers the fiber everywhere except on a spot at the center, which thus defines the active length of the probes. Based on the length of the spot, the spatial resolution is three Kolmogorov lengths in the worse case and 0.20 Kolmogorov lengths in the best one. The time response of the probes is an important issue, which is discussed, in some detail, in reference [6]. We determine it by applying square wave test; depending on the probe, the overheating, the cable length and the electronic circuitry, it varies from 3 to 16 μs, so that the frequency domain which can be explored ranges from 10 to 50 kHz . The frequency response of the probe is found acceptable for microscale Reynolds numbers ranging between 150 and 1500, over the whole range of scales — down to the dissipative range — we explore. However, in a few cases, especially for values of the Reynolds numbers larger than 1500, we have been led to apply a correction procedure, which accounts for the finite value of the time response of the probe; above 3200, we are still in position to investigate the inertial range of scales (sometimes introducing corrections), but not the dissipative one. The velocity is measured at several points, in the two set-ups. The signal is digitized on a 16 bit converter, controlled by a Digital Signal Processing card, and the ratio signal over noise of typically 70 dB. The records are of various sizes, from a few ten millions to several hundred of millions. Table I displays typical experimental conditions (here ν is the kinematic viscosity, U is the mean local velocity, u' the fluctuation (its rms value), Re is the Reynolds number based on the disk radius and the disk angular speed, R_λ is the microscale Reynolds number (based on a dissipation determined by using Howarth-Von Karman-Kolmogorov relation), λ is the Taylor scale and η the Kolmogorov scale).

Table I

Cell	ν cm^2/s	U cm/s	u' cm/s	Re	R_λ	u'/U	$\lambda(\mu$m)	$\eta(\mu$m)
2	1.6×10^{-2}	39	8	41000	151	0.20	3000	127
2	2.1×10^{-2}	284	94	2.3×10^5	674	0.33	1520	26
2	4.6×10^{-4}	128	37	4.7×10^6	2300	0.29	276	2.9
2	3.3×10^{-4}	136	52	7×10^6	5040	0.38	320	2
2	4.4×10^{-4}	128	27	5×10^6	1550	0.20	262	3.4
2	1.1×10^{-3}	64	13	2×10^6	822	0.21	680	12
1	2.7×10^{-2}	118	29	16700	188	0.25	1740	64
1	2.6×10^{-4}	27.4	6.1	4.3×10^5	879	0.22	187	5

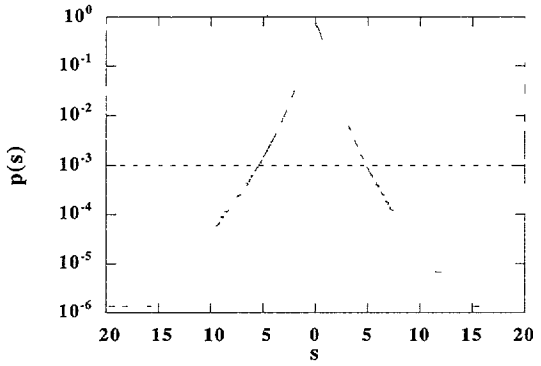

Fig. 1. — Log linear plot of the pdf of the longitudinal increments of velocity, calculated for $r = 2\eta$ (where η is the Kolmogorov length); the flow parameters are $\eta \approx 25$ μm, and $R_\lambda \approx 659$.

3. Structure of the Large Events Controlling the Tails of the pdf of the Velocity Derivative

Figure 1 shows the pdf of the velocity increments for a separation scale $r \approx 2\eta$, for $R_\lambda \approx 659$. Here, the pdf is renormalized so as to ensure that the standard deviation is equal to 1. Since r lies in the dissipative range, one can consider that the pdf of Figure 1 accurately represents the distribution of the velocity derivatives. We consider here the extreme part of the tails of such a distribution, corresponding to probability levels such that the area comprised below the tails is 2.6×10^{-3} (1.3×10^{-3} on each side of the pdf). This number has a physical interpretation: it is related to the volume fraction covered, in the physical space, by the high level velocity gradients defined above. For the particular pdf of Figure 1 the corresponding probability level is 10^{-3} (see the dashed line). We choose — somewhat arbitrarily — this threshold, because it turns out that it is difficult to identify remarkable structures from the signal at higher probability levels. Then for the rest of the paper, we shall dename the events corresponding to such parts of the tails of the pdf as corresponding to "intense" velocity gradients.

A typical "intense" event observed at small and moderate R_λ is shown in Figure 2a. The large velocity derivative takes place in the central part of this object, around $t \approx 17.8$ ms. One can see that it is embedded into a remarkable structure, which evokes the derivative of a Gaussian curve. Such structures form roughly 40% of the observed ones (the percentage given here is a very crude value). One can have other objects, less symmetric, but they have the

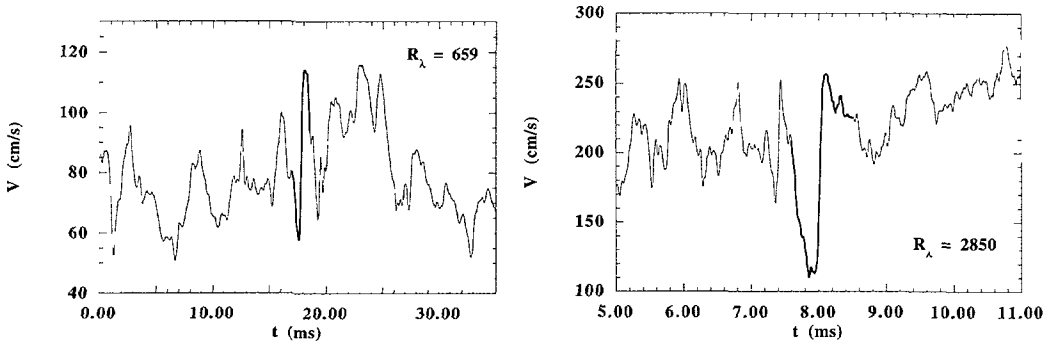

Fig. 2. — Direct time recordings for (a) $R_\lambda \approx 659$ and (b) $R_\lambda \approx 2850$; the structures which surround the large velocity derivative increment are singled out by a bold line. The time origin is arbitrary.

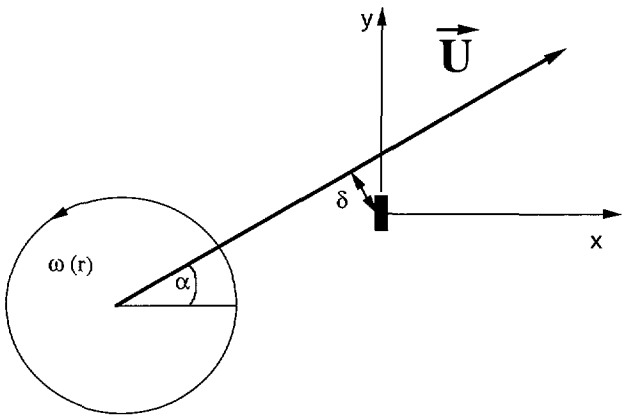

Fig. 3. — Representation of an isolated vortex filament, of axis normal to the plane (x, y), crossing the hot wire (black rectangle), at a speed U, with an angle α and a distance vortex center - probe equal to δ.

same shape. For a small part of the intense events (roughly 20%) it is difficult to identify any remarkable structure.

As mentionned above, such characteristics are observed in the lower range of Taylor Reynolds number, comprised roughly between 150 and 700. Above 700, the events have a completely different structure. This is shown in Figure 2b, where one typical event is represented. Here the large velocity derivative is located at $t \approx 8.05$ ms. In this case, the structures associated to the large events are essentially fronts preceded and followed by some rapid, small amplitude velocity fluctuations. It is difficult to define in this case a particular structure.

4. Geometrical Interpretation of the Intense Events for $R_\lambda < 700$

The event of Figure 2a can be interpreted as a Burgers type filament crossing the probe with some angle α. To show this, let us first consider a vortex filament, characterized by a vorticity field $\omega(r)$, whose axis is perpendicular to the plane (see Fig. 3); we suppose that it moves at

velocity U, with an incident angle α and that its center passes at a distance δ from the probe; α and δ completely define the impact. The hot wire (which is assumed to be parallel to y axis) can be assimilated to a point on the scale of the filament. Let us use a frame (x, y) moving with the filament, whose origin is at the vortex center; this amounts to consider that the probe moves along a straight line of equation:

$$y = x \text{ tg } \alpha - \frac{\delta}{\cos \alpha} \tag{1}$$

If we assume that the probe is sensitive only to the velocity component normal to the wire, one finds that the measured quantity $S(t)$ is:

$$S(t) = U_\theta(r)\frac{y}{r} \tag{2}$$

with $r = (x^2 + y^2)^{1/2}$ and in which (according to Taylor hypothesis), x is given by

$$x = Ut \cos \alpha \tag{3}$$

In (2), $U_\theta(r)$ is the azimuthal velocity induced by the filament, defined by:

$$\omega(r) = \frac{1}{r}\frac{\mathrm{d}(rU_\theta(r))}{\mathrm{d}r} \tag{4}$$

In the particular case where the vortex center hits the probe, we have $\delta = 0$ and therefore (3) simplifies to:

$$S(t) = U_\theta(r) \sin \alpha \tag{5}$$

In Figure 4a, we represent the vorticity field $\omega(r)$ corresponding to a Burgers vortex of radius R, intensity ω_0, defined by:

$$\omega(r) = \omega_0 \exp\left(-\frac{r^2}{2R^2}\right) \tag{6}$$

and in Figures 4b and 4c, we show the function $S(\xi)/\omega_0 R$ (where $\xi = Ut/R$, computed from (2) and (4)), for various values of δ and α. When $\delta = 0$, the expected response $S(\xi)$ is symmetric, and shows two extrema separated by a distance equal to 3.2. As δ increases, $S(\xi)$ becomes more and more asymmetric; the extreme case with $\delta = 2R$ would be rejected by our conditional sampling, which captures only the events associated to large amplitude velocity derivatives. It is remarkable that both the amplitude and the distance between the two extrema of the large events we select are almost insensitive to variations in δ. The dependence of $S(\xi)$ with the incidence angle α is shown in Figure 4c, for $\delta = 0$. It turns out that this angle essentially controls the amplitude of $S(\xi)$, without affecting its form. Here again a filament crossing the probe with a small angle would be rejected by our conditional sampling, because it does not give rise to a large velocity derivative. One may argue that the incidence angle is fairly constant, since it cannot be too small (otherwise the event is rejected), neither too large (because it is controlled by the large scale velocity fluctuations which have Gaussian distributions). A crude estimate of α, obtained directly from the signal, is $8 \pm 3°$ for a fluctuation rate of 20% [8]. As will appear below, the corresponding standard deviation of $\sin \alpha$ is smaller than that of the quantities characterizing the worms, so that this parameter can be considered as a constant. The problem of the orientation of the axis of the filament with respect to the wire requires a discussion: in particular, the fact that the worm is inclined with respect to the probe axis does not change the form of the signal which is produced, but may alter the measurement of its radius. We shall return to this point later.

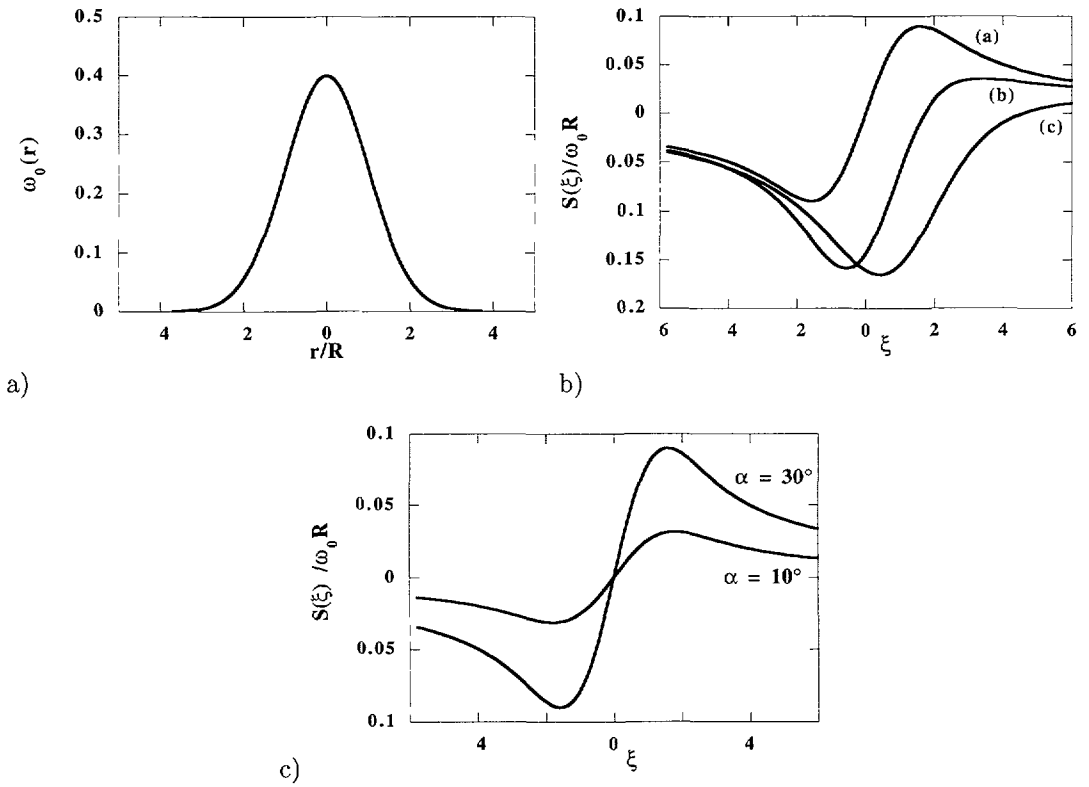

Fig. 4. — a) Vorticity profile $\omega(r)/\omega_0$ for a Burgers vortex, according to expression (6); b) $S(\xi)$ given by formula (2), for $\alpha = 0$ and different values of δ: (a) $\delta = 0$, (b) $\delta = 0.75R$, (c) $\delta = 2R$; c) $S(\xi)$ given by formula (2), for $\delta = 0$ and two different values of α.

It turns out that $S(\xi)$ shows strong similarities with the observed signal below $R_\lambda = 700$ (see Fig. 2a). The event of Figure 2a can thus be reasonably interpreted as an intense filament — called a worm — crossing the probe at some angle, with centers passing close to the sensor.

We wish to perform a *quantitative* analysis of such events; to do that, we introduce the two following quantities: Δt, the time separation between the two extrema of the observed signal. and ΔS, the corresponding peak to peak amplitude. We further assume that we have Burgers type filaments, and that their axis is normal to the plane formed by the sensor and velocity vector $\mathbf{U}$; under these conditions, the relation between these Δt, and the vortex size R is:

$$\Delta t \approx 3.2R/U \tag{7a}$$

The interpretation of ΔS is more delicate. The simplest approach is to express it in term of the maximum orthoradial velocity U_{mw} inside the filament; we thus obtain:

$$\Delta S = 2 \sin \alpha U_{\mathrm{mw}} \tag{7b}$$

We shall then use the following expressions to deduce, from the measurements of Δt and ΔS the values of R and U:

$$R = 0.31 U \Delta t \quad \text{and} \quad U_{\mathrm{mw}} = \frac{1}{2 \sin \alpha} \Delta S \tag{8}$$

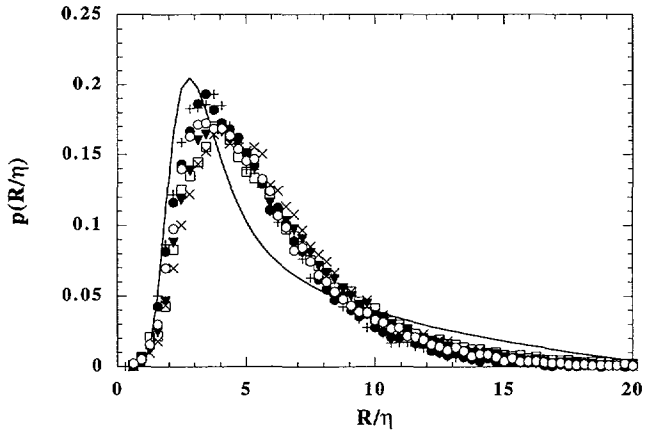

Fig. 5. — Size distributions of the worms, for different R_λ: (○) 225; (×) 151; (▼) 718; (+) 255; (●) 359; (□) 507; full line is an averaged distribution, obtained from reference [2].

and further take $\sin\alpha = 0.14$.

Now let us generalize this calculation to the case where the worms are inclined, by an angle (ϕ, ψ) with respect to the probe axis and the velocity vector **U**; we define these angles in such a way that when ϕ is zero and ψ non zero, the worm is perpendicular to **U** and shows an angle ψ with respect to the hot wire, whereas in the other case, the worm is normal to the hot wire, but shows an angle ϕ with respect to the velocity vector; ϕ and ψ would correspond to the pitch and roll angles usually defined in hot wire anemometry. The measurement is independent of the roll angle ψ, but depends on the pitch angle ϕ. Assuming a uniform distribution of pitch angles ϕ, it is possible to write a relation between the distribution of worm radius $p_0(R_w)$, and that, defined by $p(R)$, measured by the sensor: the relation reads:

$$p(R) = \frac{2}{\pi}\int_0^{\pi/2} p_0(R\cos\varphi)\mathrm{d}\varphi \tag{9}$$

We shall use this formula to interpret the distributions of worm radius we obtain. We shall not apply this approach to interpret the circulation measurements.

5. Size and Worm Reynolds Number Distributions for $R_\lambda < 700$

We first investigate the distributions of R determined by formula (8). The result is shown in Figure 5, for various values of R_λ, from 151 to 718. In Figure 5, the radii R have been rescaled by using Kolmogorov scale η, which is measured independently [7]; note that this length varies by one order of magnitude between the extreme values of R_λ shown in Figure 5. The statistics has been established over typically 25000 objects. There is some scatter, but the trend which emerges from Figure 5 is that the size distributions collapse reasonably well on a single curve for various R_λ. This result shows that the size distribution of the worms radius R is controlled by the Kolmogorov scale in this range of Reynolds numbers. It is interesting to compare such distributions with the numerical study of reference [2]. Here, we have used a fit of the numerical results of reference [2] together with formula (9) to determine the worm distribution size "seen by the probe", in a domain comprised of R/η between 0 and 20. The comparison is shown in Figure 5. Let us underline there is no adjustment factor for the R/η axis, but we

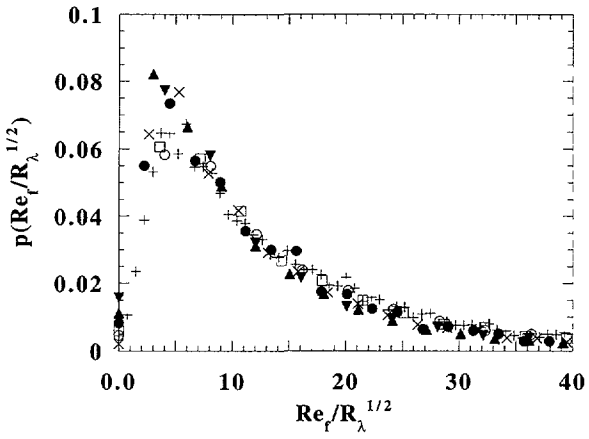

Fig. 6. — Worms Reynolds number distributions of the worms, for different R_λ: (●) 359; (+) 255; (×) 940; (○) 1342; (□) 507; (▼) 2313; (▲) 718.

have renormalized the ordinate so as to optimize the collapse between the experimental and numerical curves. Under such conditions, it is fair to say that the experimental distributions agree with the numerical one, within the error bar (the experimental error on the measurement of R, and the statistical error of Ref. [2] can be roughly estimated to 20%). One may emphasize that all the important characteristics are the same in the numerics and in the experiment: in particular, the maxima are located at the same place (the numerics is 2.8 and the experiment is 3.5) and the forms of the two distributions — numerical and experimental — are similar. Ours actually is closer to a log normal distribution than in the numerics. By determining $p_0(R/\eta)$ we can propose an experimental estimate for the mean worm size: we find $R = 3.5\ \eta$ (to be compared, in the same units to 2.8 η obtained numerically)

The distribution of the maximum internal velocity of the worm $U_{\rm mw}$ is displayed in Figure 6, for various R_λ (including values larger than 700, which we shall discuss later). In this case — for the sake of comparison with reference [2] — we use $R_{\rm f}/\sqrt{R_\lambda}$ instead of $U_{\rm mw}$, where $R_{\rm f}$ is the Reynolds number of the filament, defined by:

$$R_{\rm f} = U_{\rm mw} R/\nu,$$

in which ν is the kinematic viscosity. This number is proportional to the Reynolds number based on the circulation, introduced in reference [2]. We find that the distributions collapse reasonably well, in good agreement with the numerical findings of reference [2]. This implies, among other things, that the worm Reynolds number increases as $R_\lambda^{1/2}$, which is also in agreement with previous findings. This does not prove that this scaling accurately holds (the scatter of Fig. 6 allows other possibilities), but this shows consistency with the numerics. Thus, on the basis of the good correspondence between the size and Reynolds number distributions — in the numerics and the experiment — we may conclude that the "worms" of the numerics and the objects which we study are the same.

6. Dynamical Role of the Worms

To investigate the dynamical role of the worms, we remove them from the signal and recalculate the statistical characteristics of the system. The procedure consists in: i) detecting the worm.

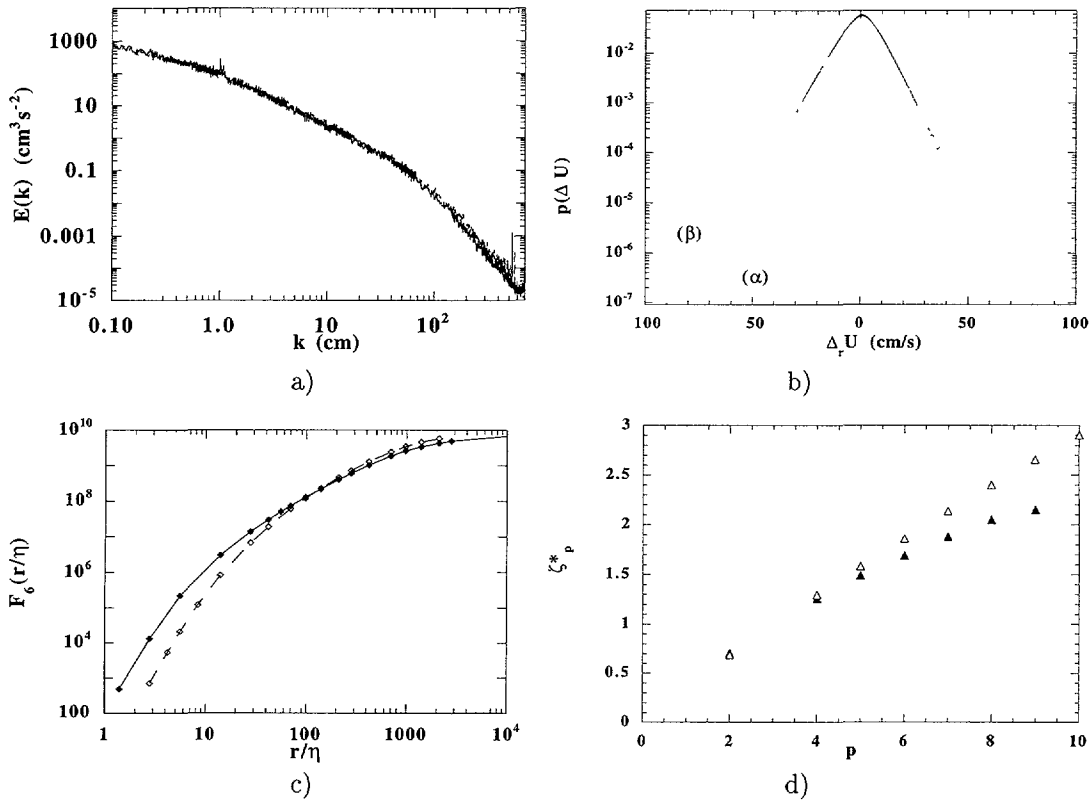

Fig. 7. — a) Energy spectrum with (dashed line) and without (full line) worms, b) Pdf of the longitudinal velocity increment for $r/\eta = 42$ ((α): without worms, (β): bare signal), c) Structure functions of order 6, with (dashed line) and without (full line) worms and d) exponents of the structure functions (black triangles: bare signal; white triangles: without worms), for $R_\lambda = 659$.

ii) tracking the positions of the velocity extrema, iii) defining a center as the middle between these two extrema, iv) defining a region, of size $9.6R$, centered on the preceding point and v) replacing the signal by a straight line, joining the two extremities of this region.

One can see that during this sort of chirurgical operation, the region we remove extends up to 4.8 times the worm radius; one may thus consider that we extract from the field not only the worms but also most of the dissipation they generate. The results are summarized in Figures 7a-d for $R_\lambda = 659$. The dashed lines correspond to the raw signal and the full lines correspond to the same signal but without worms. We recover the fact that the worms do not contribute significantly to the energy spectrum $E(k)$: the difference between the cases "with" and "without" worms is hardly visible. We have calculated that the worm contribution to the overall dissipation is 8% in this particular case. By contrast, the contribution of such objects to the intermittency in the inertial range is significant; this is visible when we inspect the tails of the pdf of the velocity increments. Figure 7b shows that on a scale comparable to Taylor scale, the sign of the curvature of the tail is inversed after the worms have been removed. The resulting pdf is closer to what we would expect if the regime was close to a Kolmogorov state. As a consequence, the high order structure functions of the inertial range are substantially modified: this is shown in Figure 7c. The difference between the two curves (with and without

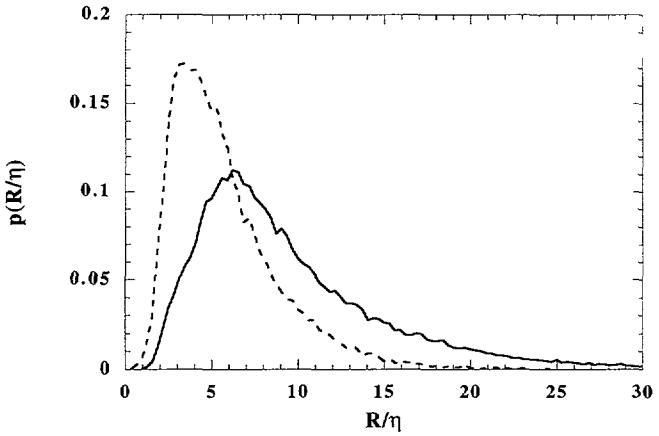

Fig. 8. — Size distributions of the worms, for $R_\lambda = 2313$ (full line); the dashed line corresponds to $R_\lambda = 225$.

worms), decreases as the scale increases, but the remarkable fact is that the worms affect the inertial range on scales much larger than their size (which are typical dissipative scales). Another consequence, already visible in Figure 7c, is that high order exponents of the structure functions are modified; this is shown in Figure 7d. The new set of exponents (i.e without worms) is now closer to the Kolmogorov value $p/3$. One may therefore conclude that the worms control a significant part (but not the totality) of the intermittency in the inertial range.

7. Size and Worm Reynolds Number Distributions for $R_\lambda > 700$

Above 700, the size distributions dramatically change. This is shown in Figure 8: here, we have plotted the size distribution using Kolmogorov units, for $R_\lambda = 2840$. One can see a dramatic change compared to Figure 8: the distribution is much wider. By contrast, no important change is observed for the circulation (See Fig. 6). It turns out that above $R_\lambda \approx 700$, the mean velocity increment across the filament decreases, while its mean radius increases so that at the end the circulation does not change. This observation may receive a simple dynamical interpretation (conservation of the circulation); all this supports the idea that above some threshold value of R_λ, those filaments become unstable, fill more space and somehow the system becomes less intermittent in the dissipative range; it is thus not so surprising to find that above the same threshold, the skewness and the flatness of the velocity derivatives cease to increase, as shown in a previous study on the same system [6].

8. Conclusion

To summarize, we have shown that the events which compose the extreme parts of the tails of pdf of the velocity derivative have a remarkable structure below some threshold value of R_λ which we roughly estimate to 700. Below this threshold, the structure of such events can be reasonably well associated to intense Burgers type vortices — denamed as worms in reference [2]. To explore their dynamical role, we remove them from the field, by "treating" a region, centered around the worm, of size equal to 4.8 times the core diameter; if the worm

is a Burgers type vortex, this "ablation" includes both the core and most of the dissipation associated to it. It turns out that we recover earlier results i.e the worms contribute only little to the overall dissipation. This fact is interesting in itself, and is consistent with previous work on the subject [2]. However, the striking result we find is that the worms control a significant part of the intermittency in the inertial range. The fact that worms (which are dissipative objects if we consider their diameter) affect inertial range quantities can be viewed as a finite Reynolds effect: at much larger Reynolds numbers, one would expect that their influence becomes negligible in the major part of the inertial range; actually, the present experiment suggests that we are still far away from such a state, even at the largest Reynolds number we can achieve.

Above 700, we observe an abrupt structural change which evokes the onset of an instability. These results allow to offer a physical interpretation of previous observations made on the skewness and flatness of the velocity derivatives [6], and may also answer a question previously raised on the stability of such objects as R_λ increases [2]. They support the general view that we have to achieve extremely high Reynolds numbers to reach an asymptotic state, where all such objects might be somehow completely "dissolved" in the background. They also show that it is instructive to investigate the structure of small scale objects on the raw velocity signal in addition to determining statistical quantities. This is not really new in the context of turbulence [9]: to be specific, a similar approach has been undertaken in a mixing layer some years ago [10], and more recently on local pressure measurements performed between counter-rotating disks [11]; so far actually, no systematic tracking of structures in the *dissipative range*, has been carried out, from the *velocity* signal, in turbulent flows. We tend to believe that it would be instructive to develop such an approach, more systematically, in other turbulent systems.

Acknowledgments

The authors are grateful to O. Cadot, Y. Couder, S. Douady, A. Pravkowsky, R Benzi, J. Jimenez for interesting discussions related to this experiment. This work has been supported by CNRS, Universities Paris VI and Paris VII, École Normale Supérieure.

References

[1] See for instance a recent review by Nelkin M., *Adv. Phys.* **43** (1994) 143.
[2] Jimenez J., Wray A.A., Saffman P.G. and Rogallo R.S., *J. Fluid Mech.* **65** (1993) 255.
[3] Douady S., Couder Y. and Brachet M.E., *Phys. Rev. Lett.* **67** (1991) 983; Douady S. and Couder Y., in "Turbulence in Extended Systems", R. Benzi, C. Basdevant and S. Ciliberto, Eds. (Nova Science Publishers, 1993) pp. 3-17.
[4] Fauve S., Laroche C. and Castaing B., *J. Phys. II France* **3** (1993) 271.
[5] Cadot O., Douady S. and Couder Y., *Phys. Fluids* **7** (1995).
[6] Tabeling P., Zocchi G., Belin F., Maurer J. and Willaime H., to appear in *Phys. Rev. E.*
[7] Maurer J., Tabeling P. and Zocchi G., *Europhys. Lett.* **26** (1994) 31; Zocchi G., Maurer J., Tabeling P. and Willaime H., *Phys. Rev. E* **50** (1994) 3693.
[8] α, and its standard deviation, are estimated from the distribution of the velocity of the vortex center, together with the hypothesis that the transverse component is 100% of the longitudinal one (note that this number is probably excessive for a mixing layer).

[9] After Brown and Roskho's experiment (Brown G.L. and Roshko A., *J. Fluid. Mech.* **65** (1974) 775) a considerable amount of studies have been carried out to identify, from local velocity measurements, large scale structures in turbulent flows. Here we are concerned only with small scale structures, several Kolmogorov lengths in size.

[10] Jimenez, private communication. See also Huang L.S. and Ho C.M., *J. Fluid. Mech.* **210** (1990) 475.

[11] Abry P., Fauve S., Flandrin P. and Laroche C., *J. Phys. II France* **4** (1994) 725; see also [5].